Piezoelectric Properties of Zinc Oxide Thin Films Grown by Plasma-Enhanced Atomic Layer Deposition

Taher Abu Ali, Julian Pilz, Philipp Schäffner, Markus Kratzer, Christian Teichert, Barbara Stadlober, and Anna Maria Coclite*

Zinc oxide (ZnO) thin films are deposited by plasma-enhanced atomic layer deposition (PE-ALD). This deposition method allows depositing stoichiometric and highly resistive ZnO films at room temperature. Despite such important requirements for piezoelectricity being met, not much is known in literature about the piezoelectric properties of ZnO thin films (<70 nm) deposited by PE-ALD. The films are grown at different substrate temperatures to investigate the effect on crystalline and piezoelectric properties. Films deposited on flexible poly(ethylene terephthalate) (PET) generated a higher piezoelectric current (>1.8 nA) and charge (>80 pC) compared with films deposited on glass (>0.3 nA and >30 pC) due to bending effects of the substrate when mechanically excited. Furthermore, increasing the substrate temperature, during deposition, enhances the growth along the (002) crystallographic orientation, which further strengthens the generated piezoelectric current signal for mechanical excitations along the ZnO film's *c*-axis.

1. Introduction

Zinc oxide (ZnO) has attracted a lot of interest in material research due to its wide bandgap energy (3.37 eV),[1] high excitonic binding energy (60 mV),[2] and relatively high piezoelectric coefficients ($d_{33} = 11.67$ pC N^{-1} and $d_{31} = -5.43$ pC N^{-1}, for

T. Abu Ali, Dr. J. Pilz, Prof. A. M. Coclite
Institute of Solid State Physics
NAWI Graz
Graz University of Technology
Petersgasse 16, 8010 Graz, Austria
E-mail: anna.coclite@tugraz.at

T. Abu Ali, P. Schäffner, Dr. B. Stadlober
MATERIALS-Institute for Surface Technologies and Photonics
Joanneum Research Forschungsgesellschaft mbH
Franz-Pichler-Str. 30, 8160 Weiz, Austria

Dr. M. Kratzer, Prof. C. Teichert
Institute of Physics
Montanuniversität Leoben
Franz Josef Str. 18, 8700 Leoben, Austria

The ORCID identification number(s) for the author(s) of this article can be found under https://doi.org/10.1002/pssa.202000319.

bulk ZnO).[3] Such properties, associated with its wurtzite structure, make ZnO of particular interest in many applications which include electronics (transparent electrodes and transparent thin-film transistors),[1,4] optoelectronics (laser diodes and solar cells),[2,5] sensors (chemical, piezoelectric, and pyroelectric),[6,7] transducers (surface acoustic wave devices),[8] and energy harvesting.[9] In addition, ZnO is an n-type semiconductor, where its semiconducting properties are tuned by doping, annealing, and most importantly by the growth process and related process parameters.[10–13] Therefore, several techniques have been implemented to synthesize ZnO bulk crystals or films and tailor their properties for different applications.[10] Of particular interest is atomic layer deposition (ALD).[14] It allows the deposition of uniform and conformal ZnO thin films with Å-level precision.[14,15] Uniformity and conformality are products of self-limiting layer-by-layer film growth from vapor-phase precursors, with each precursor dosing step being separated by a purging step. Common ALD processes include thermal ALD and plasma-enhanced ALD (PE-ALD). PE-ALD allows for the deposition of high-quality films at lower substrate temperatures compared with thermal ALD as the surface reactions are driven by energetic plasma species rather than thermal energy.[16] Such low-deposition temperatures are suitable for ZnO growth on flexible substrates such as polymers, while maintaining control over films' optical, electrical, and mechanical properties.[17,18]

Similarly, the piezoelectric properties of ZnO films are influenced by the deposition technique and the growth parameters. **Table 1** shows the piezoelectric coefficient d_{33} of ZnO films prepared by several deposition techniques as reported in literature.

The investigation of the piezoelectric properties in these studies was conducted by piezoresponse force microscopy (PFM), which measures the indirect piezoelectric effect, i.e., the reported values result from a local microscopic effect.[24–26] Macroscopic piezoelectric properties can be measured with a stamp setup, which excites the piezoelectric material mechanically and measures the direct piezoelectric effect.

While piezoelectric characterization has been reported for ZnO films grown by different techniques, the literature on piezoelectric properties of ZnO films prepared by ALD is very limited.[27,28] Nevertheless, ZnO deposited by ALD and especially PE-ALD has shown ideal properties for piezoelectric

Table 1. Reported piezoelectric coefficient d_{33} of ZnO films.

Technique	Film thickness [nm]	d_{33} [pm V^{-1}]
Pulsed laser deposition (PLD)	200	12[19]
PLD	50	25[20]
PLD	800	49.7[21]
Radio frequency (RF) magnetron sputtering	285	5[22]
RF magnetron sputtering	710	5.3[22]
RF magnetron sputtering	1400	8[22]
Direct current sputtering	210	110[23]

applications such as polycrystallinity with (002) texture,[18,29,30] high resistivity,[18,29] and a low amount of impurities.[17,29,31,32] Furthermore, the high reactivity of the plasma coreactant allows for the deposition on thermosensitive substrates at substrate temperatures as low as room temperature.[17,18] This study therefore focuses on the piezoelectric properties of ZnO thin films grown on flexible PET and rigid glass substrates at different substrate temperatures.

2. Results

As the crystallographic properties have a large effect on the piezoelectric coefficients,[33,34] X-ray diffraction (XRD) was performed. The XRD spectra of ZnO thin films grown on PET/ITO and on glass/ITO at different substrate temperatures is shown in **Figure 1**a,b, respectively. The spectra are shown in a 2θ range in which the highest-intensity peaks corresponding to the ZnO wurtzite structure were observed (low-intensity peaks corresponding to the (110) and (103) crystallographic orientation can be observed at higher angles, cf. Figure S1, Supporting Information). For all the measured spectra in Figure 1a,b, a decaying background can be observed, which can be associated with the amorphous substrate. The ZnO samples show a polycrystalline pattern with diffraction peaks which can be associated with the (100) and (002) crystallographic orientation of the ZnO wurtzite structure. By increasing the substrate temperature, the preferential orientation of the films switches from (100) to (002). By further increase in substrate temperature beyond 150 °C, the contribution from the (100) orientation further diminishes. Furthermore, the (002) peak position shifts to higher angles with increased substrate temperature, mainly for the samples deposited on PET/ITO, which could be explained by decreased microstrain within the sample. As the c-axis is the polar axis in the hexagonal wurtzite structure, a strong (002) preferential orientation of the crystallites is desired to enhance the measured piezoelectric current.[17,18,22,35,36]

The piezoelectric current signal I was measured as a function of time t upon periodic force cycles applied to ZnO thin films by means of the setup shown in **Figure 2**.

Figure 3 shows the characteristic output plots for the films deposited at 25 °C a) on the ITO-coated PET substrate and b) on ITO-coated glass substrate. Positive current pulses are generated upon pressing onto the sample and negative current pulses upon releasing the stamp from the sample. For such films, the average positive piezoelectric peak current generated
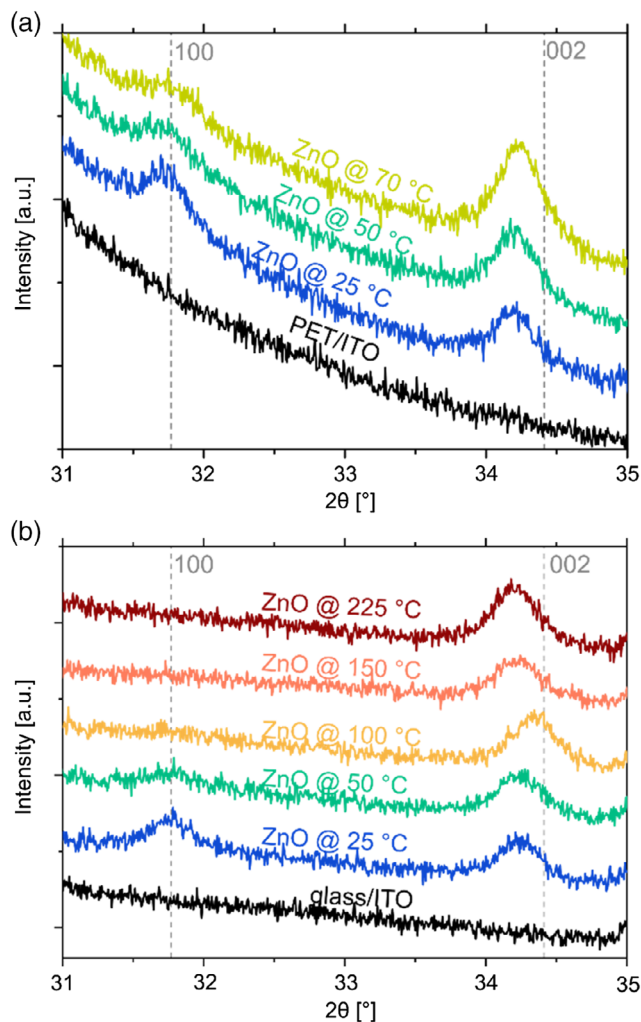

Figure 1. XRD patterns of ZnO films grown a) on PET/ITO and b) on glass/ITO at different substrate temperatures. Vertical, dashed lines show the peak positions of a ZnO powder reference (ICSD-26170).[37] Patterns are stacked for clarity.
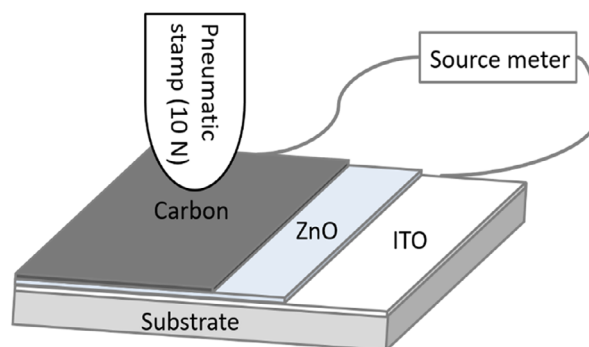

Figure 2. Schematic diagram of device architecture and piezoelectric measurement setup. Image not to scale, the area of the tip is 0.8 cm^2 and the sample size is 1.5 cm^2.

from one cycle was 1.8 ± 0.1 nA when deposited on PET and 0.3 ± 0.1 nA when deposited on glass. When the films deposited

ADVANCED
SCIENCE NEWS
www.advancedsciencenews.com

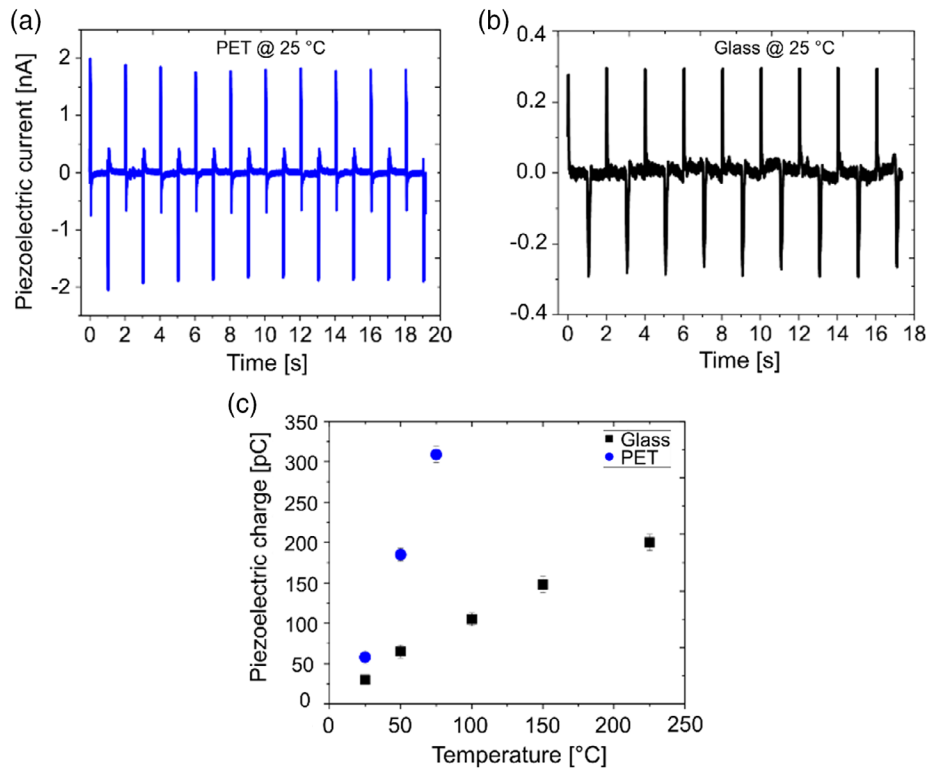physica pssa
status solidi
www.pss-a.com

Figure 3. Piezoelectric current signal versus time for 9–10 step force cycles applied to ZnO thin films deposited at 25 °C a) on ITO-coated PET and b) on ITO-coated glass. c) Generated piezoelectric charge as a function of the substrate deposition temperature for films grown on PET and glass.

on PET/ITO were mechanically excited, a recoil current was detected upon pressing and releasing, due to the elasticity of the substrate.[38] The piezoelectric charge Q was calculated by integrating the piezoelectric current over time, as shown in Equation (1).

$$Q = \int I dt \tag{1}$$

Figure 3c shows the calculated piezoelectric charge Q for ZnO thin films deposited on both flexible PET and rigid glass substrates at different substrate temperatures T, respectively. A linear increase in piezoelectric charge for films on both substrates was observed. For ZnO on PET, with increasing substrate temperature to 50 °C resulted in a piezoelectric peak current of $I = 3.6 \pm 0.1$ nA, corresponding to a charge of $Q = 180 \pm 10$ pC. Further increase of the substrate temperature to 70 °C resulted in a piezoelectric peak current of $I = 5.8 \pm 0.1$ nA and $Q = 320 \pm 10$ pC. The increasing linear trend, attributed to the enhancement of the (002) orientation with increased temperature, was measured also for the samples deposited on glass: in this case, at 50 °C, the generated piezoelectric peak current was $I = 1.4 \pm 0.2$ nA and $Q = 65 \pm 8$ pC. It reached a maximum of 4.3 ± 0.2 nA ($Q = 190 \pm 10$ pC) for samples deposited at 225 °C.

Piezoelectric current/charge generated from ZnO thin films deposited on rigid glass substrates was lower compared with those generated by ZnO thin films on flexible PET substrates, due to bending effects of the substrate.[39] Bending of PET substrates generates charges through the transverse piezoelectric

effect (attributed to the d_{31} coefficient), which results in a higher measured piezoelectric current/charge.[40] However, ZnO films deposited on rigid glass substrates are not prone to bending, resulting in lower generated piezoelectric current/charge. As the response of ZnO films deposited on glass is not expected to have d_{31} contributions, the piezoelectric coefficient d_{33} can be calculated by

$$d_{33} = Q/F \tag{2}$$

where Q is the piezoelectric charge and F is the excitation force. The calculated d_{33} coefficients are shown in **Table 2**.

The calculated piezoelectric coefficient ranges between 3.0 and 20.0 pC N^{-1}, for ZnO films grown within the temperature range of 25 to 225 °C. The d_{33} values are comparable with thicker films obtained by other deposition techniques such as sputtering (see Table 1) as well as bulk ZnO ($d_{33} = 11.67$ pC N^{-1}),[3]

Table 2. Calculated piezoelectric coefficient for ZnO films deposited on glass substrates at different temperatures.

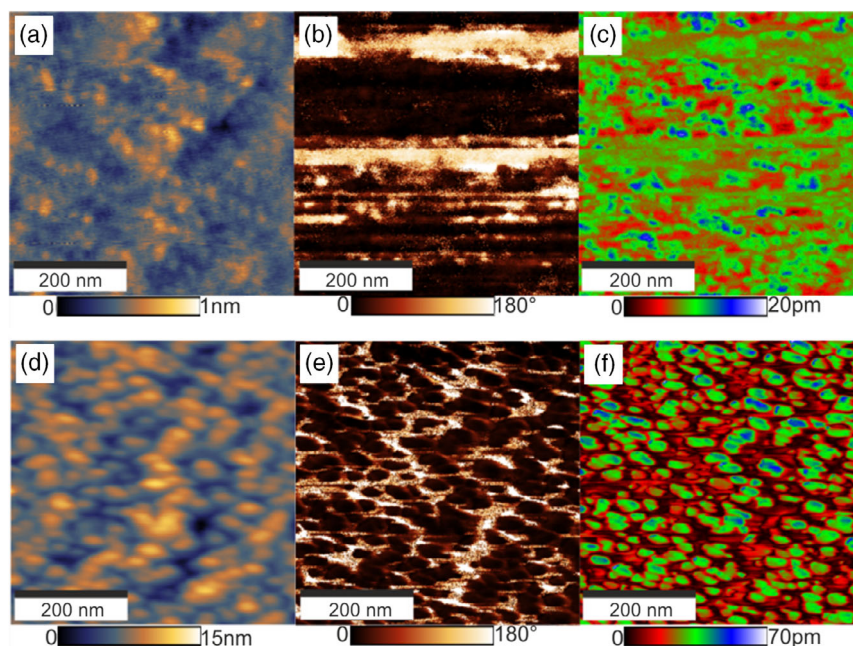| Deposition temperature [°C]	d_{33} [pC N^{-1}]
25	3.0
50	6.5
100	10.5
150	14.8
225	20.0

Figure 4. a) Topography, b) PR phase, c) PR amplitude of ZnO at 25 °C, d) topography, e) PR phase, and f) PR amplitude of ZnO at 225 °C. Both films are grown on Si substrates.

which shows that PE-ALD is a promising technique for the deposition of piezoelectric ZnO films. Furthermore, while the piezoelectric output of (thermal) ALD ZnO layers has been investigated, no d_{33} coefficients have been reported in these studies.[27,28]

The results obtained from our in-house-built piezoelectric setup allows macroscopic piezoelectric characterization of ZnO thin films. However, microscopic characterization using PFM gives information about the local piezoelectric properties at a nanometer scale. **Figure 4**a shows the topography of the ZnO film deposited at 25 °C, which is characterized by small grains <30 nm. The phase response (Figure 4b) does not show a coherent orientation of grain polarization. However, large areas are recognizable, where the piezoelectric phase is ≈180°. The piezoresponse (PR) amplitude (Figure 4c) is relatively low, with a maximum displacement of 20 pm. The incoherence of the phase response and the low amplitude can be explained by the crystallographic properties of the film, i.e., where the wurtzite ZnO structure is mostly oriented along the (100) axis. Figure 4d shows the topography of ZnO film deposited at 225 °C, which is characterized by granular topography with grain diameter of ≈60 nm. The PR amplitude signal (Figure 4f) follows the grain structure, where regions with higher piezoelectric displacements are mostly located within the grains, whereas at the grain boundaries, the displacement is lower. This could be attributed to the fact that the grain boundaries are crystallographic defects. From the PFM phase image (Figure 4e), a certain degree of phase shift is recognizable. The grains seem to be in phase with the external AC driving voltage, whereas boundaries seem to be mostly out of phase. Considering that the wurtzite ZnO structure in this film is mostly oriented along the (002) axis, the PFM phase can be related with grain polarization, and this being in phase, it corresponds to a Zn-terminating surface.

3. Conclusion

Piezoelectricity in ZnO thin films deposited on flexible PET substrates as well as on rigid glass substrates by PE-ALD at different substrate temperatures was investigated. For this purpose, the piezoelectric current/charge was macroscopically measured and evaluated with an in-house-built piezoelectric measurement setup, applying a periodic step force signal of 10 N. ZnO films grown on flexible substrates showed increased piezoelectric output (up to 320 pC) compared with films grown on rigid substrates, possibly due to contributing bending effects upon force application. Furthermore, films showed increased piezoelectric output with increasing substrate temperature for both substrates, which can be related to an enhanced orientation of the crystallites along the polar (002) crystallographic axis. This is confirmed by PFM measurements which indicate a predominant polarization orientation in the film.

4. Experimental Section

ZnO thin films were grown by PE-ALD in an in-house-built direct plasma reactor. Details on the setup can be found in previous studies.[17,18] One cycle of the process consisted of 0.15 s diethylzinc (DEZ) dose, 22 s Argon (Ar) purge, 8 s O₂–plasma (60 W power), and 15 s Ar purge. ZnO films were deposited on Si (100) wafers with native oxide (Siegert Wafer, cut to ≈2 × 2 cm) for spectroscopic ellipsometry (SE) and PFM measurements and on PET coated with indium tin oxide (ITO; 60 Ω sq⁻¹ surface resistivity) substrates (Sigma-Aldrich, Germany), as well as glass coated with ITO (60 Ω sq⁻¹ surface resistivity) substrates (Sigma-Aldrich, Germany) for crystallographic and macroscopic piezoelectric characterization. Depositions on ITO-coated PET substrates were conducted at substrate temperatures of 25, 50, and 70 °C. Due to the temperature-dependent growth per cycle of the ALD process,[14] the number of cycles was adapted for each deposition series to reach a thickness of around 65 nm.

Depositions on ITO-coated glass substrates were conducted at 25, 50, 100, 150, and 225 °C with resultant film thicknesses of around 50 nm.

SE (J.A. Woollam M-2000V) was conducted on films grown on Si substrates to determine the thickness and optical constants of the films. Measurements were carried out in a wavelength range of 370–1000 nm at three different angles (65°, 70°, and 75°). Using a Cauchy model in the transparent region of the ZnO films (450–1000 nm), the thickness and refractive index of the films were extracted.

XRD in a θ/θ configuration (Panalytical Empyrean) was conducted to analyze the specular crystal orientation of films grown on PET/ITO substrates, as well as films grown on glass/ITO substrates. A 1/8° divergence slit, a 4 mm mask, and a P7.5 antiscatter slit were used in the setup, and the detector was operated in the 1D mode.

The macroscopic piezoelectric properties were measured in an in-house-built piezoelectric measurement setup. For this evaluation, conductive carbon tape (Science Services GmbH) was applied on the ZnO film, as a top electrode. The setup consisted of a pneumatic stamp generating a step force signal with magnitude $F = 10\,N$ and frequency $f = 0.5\,Hz$. The generated piezoelectric current I was measured with a National Instruments PXIe-4139 source meter, for 9–10 cycles of step force. Piezoelectric charge Q values were calculated from the integrated current signal.

To confirm the trends of the macroscopic measurements, PFM measurements were carried out on ZnO films grown on Si. The measurements were conducted utilizing an Asylum Research (Oxford Instruments) MFP 3D atomic force microscope using a Ti-/Ir-coated ASYLELEC-01-R2 conductive probe with a nominal tip radius of (25 ± 10) nm and a cantilever spring constant of 2.8 (1.4–5.8) Nm^{-1}. To extend the applicable voltage range, a 10 × voltage amplifier F10A from FLC Electronics AB was interconnected between the atomic force microscopy (AFM) controller output and the AFM probe. For signal enhancement, the measurements were carried out in the Dual AC Resonance Tracking (DART) mode, exploiting the superior signal-to-noise ratio enhancement at contact resonance.[41]

Supporting Information

Supporting Information is available from the Wiley Online Library or from the author.

Acknowledgements

Conflict of Interest

The authors declare no conflict of interest.

Keywords

[1] H. W. Huang, W. C. Chang, S. J. Lin, Y. L. Chueh, *J. Appl. Phys.* **2012**, *112*, 124102.

[2] M. Jin, J. Jo, G. P. Neupane, J. Kim, K. S. An, J.-W. Yoo, *AIP Adv.* **2013**, *3*, 102114.

[3] Y. Lu, N. W. Emanetoglu, Y. Chen, in *Zinc Oxide Bulk, Thin Films and Nanostructures*, Elsevier, Oxford **2006**, pp. 443–489.

[4] K. Park, D. K. Lee, B. S. Kim, H. Jeon, N. E. Lee, D. Whang, H. J. Lee, Y. J. Kim, J. H. Ahn, *Adv. Funct. Mater.* **2010**, *20*, 3577.

[5] H. K. Liang, S. F. Yu, H. Y. Yang, *Appl. Phys. Lett.* **2010**, *97*, 241107.

[6] L. Zhu, W. Zeng, *Sens. Actuators A* **2017**, *267*, 242.

[7] C. C. Hsiao, K. Y. Huang, Y. C. Hu, *Sensors* **2008**, *8*, 185.

[8] J. Chen, X. He, W. Wang, W. Xuan, J. Zhou, X. Wang, S. R. Dong, S. Garner, P. Cimo, J. K. Luo, *J. Mater. Chem. C*, **2014**, *2*, 9109.

[9] Z. L. Wang, J. Song, *Science* **2006**, *312*, 242.

[10] Ü. Özgür, Y. I. Alivov, C. Liu, A. Teke, M. A. Reshchikov, S. Doğan, V. Avrutin, S. J. Cho, H. Morkç, *J. Appl. Phys.* **2005**, *98*, 1.

[11] A. Perrotta, J. Pilz, A. Milella, A. M. Coclite, *Appl. Surf. Sci.*, **2019**, *483*, 10.

[12] M. A. Thomas, J. B. Cui, *ACS Appl. Mater. Interfaces* **2012**, *4*, 3122.

[13] E. Guziewicz, M. Godlewski, L. Wachnicki, T. A. Krajewski, G. Luka, S. Gieraltowska, R. Jakiela, A. Stonert, W. Lisowski, M. Krawczyk, J. W. Sobczak, A. Jablonski, *Semicond. Sci. Technol.* **2012**, *27*, 074011.

[14] T. Tynell, M. Karppinen, *Semicond. Sci. Technol.* **2014**, *29*, 043001.

[15] S. M. George, *Chem. Rev.* **2010**, *110*, 111.

[16] H. B. Profijt, S. E. Potts, M. C. M. van de Sanden, W. M. M. Kessels, *J. Vac. Sci. Technol. A* **2011**, *29*, 050801.

[17] J. Pilz, A. Perrotta, P. Christian, M. Tazreiter, R. Resel, G. Leising, T. Griesser, A. M. Coclite, *J. Vac. Sci. Technol. A* **2018**, *36*, 01A109.

[18] J. Pilz, A. Perrotta, G. Leising, A. M. Coclite, *Phys. Status Solidi* **2019**, *217*, 1900256.

[19] I. K. Bdikin, J. Gracio, R. Ayouchi, R. Schwarz, A. L. Kholkin, *Nanotechnology* **2010**, *21*, 235703.

[20] D. D'Agostino, C. Di Giorgio, A. Di Trolio, A. Guarino, A. M. Cucolo, A. Vecchione, F. Bobba, *AIP Adv.* **2017**, *7*, 055010.

[21] W. Qin, T. Li, Y. Li, J. Qiu, X. Ma, X. Chen, X. Hu, W. Zhang, *Appl. Surf. Sci.* **2016**, *364*, 670.

[22] M. Laurenti, S. Stassi, M. Lorenzoni, M. Fontana, G. Canavese, V. Cauda, C. F. Pirri, *Nanotechnology* **2015**, *26*, 215704.

[23] Y. C. Yang, C. Song, X. H. Wang, F. Zeng, F. Pan, *Appl. Phys. Lett.* **2008**, *92*, 012907.

[24] M. Kratzer, M. Lasnik, S. Röhrig, C. Teichert, M. Deluca, *Sci. Rep.* **2018**, *8*, 1.

[25] O. Kolosov, *Phys. Rev. Lett.* **1996**, *76*, 4292.

[26] E. Soergel, *J. Phys. D: Appl. Phys.* **2011**, *44*, 464003.

[27] L. Y. Zhu, J. G. Yang, K. Yuan, H. Y. Chen, T. Wang, H. P. Ma, W. Huang, H. L. Lu, D. W. Zhang, *APL Mater.* **2018**, *6*, 121109.

[28] B. S. Blagoev, M. Aleksandrova, P. Terziyska, P. Tzvetkov, D. Kovacheva, G. Kolev, V. Mehandzhiev, K. Denishev, D. Dimitrov, *J. Phys. Conf. Ser.* **2018**, *992*, 012027.

[29] D. Kim, H. Kang, J. M. Kim, H. Kim, *Appl. Surf. Sci.* **2011**, *257*, 3776.

[30] S. H. K. Park, C. S. Hwang, H. S. Kwack, J. H. Lee, H. Y. Chu, *Electrochem. Solid-State Lett.* **2006**, *9*, G299.

[31] P. C. Rowlette, C. G. Allen, O. B. Bromley, A. E. Dubetz, C. A. Wolden, *Chem. Vap. Depos.* **2009**, *15*, 15.

[32] J. Zhang, H. Yang, Q. Zhang, S. Dong, J. K. Luo, *Appl. Surf. Sci.* **2013**, *282*, 390.

[33] B. Liu, M. Wang, M. Chen, J. Wang, J. Liu, D. Hu, S. Liu, X. Yao, H. Yang, *ACS Appl. Mater. Interfaces*, **2019**, *11*, 12656.

[34] J. G. E. Gardeniers, Z. M. Rittersma, G. J. Burger, *J. Appl. Phys.* **1998**, *83*, 7844.

[35] N. J. Blumenstein, F. Streb, S. Walheim, T. Schimmel, Z. Burghard, J. Bill, *Beilstein J. Nanotechnol.* **2017**, *8*, 296.

[36] S. J. Kang, Y. H. Joung, *Appl. Surf. Sci.* **2007**, *253*, 7330.

[37] S. C. Abrahams, J. L. Bernstein, *Struct. Crystallogr. Cryst. Chem.* **1969**, *25*, 1233.

[38] S. Park, H. Kim, M. Vosgueritchian, S. Cheon, H. Kim, J. H. Koo, T. R. Kim, S. Lee, G. Schwartz, H. Chang, Z. Bao, *Adv. Mater.* **2014**, *26*, 7324.

[39] X. Yan, W. Ren, H. Xin, P. Shi, X. Chen, X. Wu, *Ceram. Int.* **2013**, *39*, S583.

[40] G. J. T. Leighton, Z. Huang, *Smart Mater. Struct.* **2010**, *19*, 065011.

[41] B. J. Rodriguez, C. Callahan, S. V. Kalinin, R. Proksch, *Nanotechnology* **2007**, *18*, 475504.